PAPER

Check for updates

Enhanced adsorption-based atmospheric water harvesting using a photothermal cotton rod for freshwater production in cold climates†

Wenchang Zhang,[ab] Yu Xia,[c] Zhaotong Wen,[b] Wenxia Han,[a] Shaofu Wang,[c] Yiping Cao, [b] Rong-Xiang He,[b] Yumin Liu [b] and Bolei Chen [*ab]

Solar energy-powered adsorption-based atmospheric water harvesting (ABAWH) is an emerging technology for freshwater production, especially in water-scarce regions that are remote and landlocked. Numerous water adsorbents have been used in ABAWH devices to convert molecule to liquid water. However, it is still challenging to harvest water from the air in cold winter, owing to the water adsorption of sorbents decreasing significantly at low temperature. Herein, we designed and fabricated an ABAWH device by integrating composited ionic liquids (CILs) with carbon nanotubes (CNTs) photothermal materials on the surface of cotton rod fibers. CILs extract water from the air. CNTs enable light-to-heat conversion and drive the solar evaporation process. Importantly, the cotton rods offer a backbone porous structure to maintain its internal temperature at 20 °C under solar irradiation, and thus promote the water adsorption performance of CILs at low environmental temperature. Freshwater is successfully harvested under environment temperature of 6 °C, 30% RH and solar irradiation intensity of 0.6 kW m^{-2}. The water yield can achieve 1.49 kg per m^2 per day in an outdoor environment. We believe that the ABAWH device offers a promising approach to effectively harvest water from the air at low temperature and humidity conditions.

1. Introduction

Producing affordable freshwater has been considered a global challenge facing modern society.[1–3] Two-thirds of the world's population will be under water stress conditions, according to the report of the United Nations (UN) and World Health Organization (WHO).[4] Water sources are not evenly distributed across the globe, especially in large parts of Africa, Asia and Europe.[5] This issue has become worse recently in most of the inland area due to reduced river flow and shrinking lakes, which are caused by the global climate change.[6] Moreover, the freshwater shortage occurs at high latitudes in winter, such as north of China.[5,7] A slower hydrologic cycle, including less evapotranspiration, frozen surface water and reduced rainfall, exacerbates the situation.[8] So, the individual and public health in those areas are under threat due to the shortage of clean water. To address the issue of freshwater shortage, various advanced materials and techniques have been developed for harvesting freshwater from the sea,[9,10] underground water[11] and polluted water,[12] including reverse osmosis and low-temperature multiple-effect distillation.[13] However, the application of these techniques are still limited because of their high energy consumption and the inevitable need of water sources, particularly in areas that are neither close to any surface water or sea nor having groundwater conditions.[4,14] Considering the fact that there are about 12 900 billion tons of water stored in the atmosphere, several atmospheric water harvesting (AWH) technologies have been investigated for freshwater production in the past ten years.[15–17] For instance, fog and dew harvesting is an attractive passive way that involves the collection of droplets from atmospheric water by condensation. However, it is only available when the ambient relative humidity (RH) is near 100%.[18–20]

In the following years, the active adsorption-based AWH (ABAWH) with solar-driven interfacial evaporation was rapidly developed to overcome the limitation of passive methods in low RH environment.[6,16,21] This technology is composed of three parts, including atmospheric water adsorption, water desorption through photothermal interface and collection of condensates. The absorption process takes place at night and the desorption process comes up during the daytime.[22] One approach towards ABAWH is designed based on metal–organic framework (MOF) materials.[23–25] The MOF photothermal materials worked as a solar absorber and extracted atmospheric

[a]Hubei Key Laboratory of Environmental and Health Effects of Persistent Toxic Substances, School of Environment and Health, Jianghan University, Wuhan, 430056, P. R. China. E-mail: bl_chen@jhun.edu.cn

[b]Institute for Interdisciplinary Research (IIR), Jianghan University, Wuhan 430056, P. R. China

[c]School of Physics and Technology, Key Laboratory of Artificial Micro/Nano Structures, Ministry of Education, Wuhan University, Wuhan 430072, P. R. China

† Electronic supplementary information (ESI) available. See DOI: 10.1039/d1ra06987j

water from the air at night, while they desorbed water steam under solar irradiation. The devices can work under extreme environment even in the desert. Hybrid hygroscopic aerogels are also used to fabricate ABAWH device.[26–28] The deliquescent salts, such as LiCl and CaCl$_2$, were usually loaded in the aerogel and worked as water absorbers from the atmosphere.[4,14,15,29] Recently, liquid sorbents (including ionic liquids and salt solution) were employed to assemble the ABAWH device because of their advantages (such as more durability) and in terms of their system continuity, compared with most of the solid water sorbents.[30,31] Notably, ionic liquids (ILs) can extract water from the air over a wider range of humidity values than other liquid sorbents.[30] The considerable adsorption performance is attributed to the hydrogen bonds between the anions and water molecules.[32–35] Thus, an ABAWH device based on water sorbents offers a promising approach to solve the issue of freshwater shortage in most of the inland areas. Despite the advances in ABAWH devices, the harvesting of freshwater from the air is still challenging in the winter at high latitudes. Considering that atmospheric sorbents extract molecules directly from the air, the performance of water sorbents may decrease significantly at low environmental temperature.[31,35] Indeed, it is desirable to design and fabricate a novel ABAWH device that can produce freshwater in cold winter from the air.

Herein, we designed and fabricated an ABAWH device based on the commercial cotton rod, which can harvest freshwater from air under solar irradiation at environmental temperatures below 10 °C (Fig. 1). The device is composed of a CILs sorbent, a solar absorber and a water collector. The CILs sorbent is a mixture of ionic liquids (1-hydroxyethyl-3-methylimidazolium

chloride, [C$_2$OHmim]Cl) and lithium chloride (LiCl). The solar absorber is assembled by commercial cotton rods modified with a dip-and-dry coating of CNTs (CNTs-CILs@cotton rod). Moreover, the modified cotton rods offer a porous matrix for confining the CILs sorbent. A home-made glass substrate is used to collect water by condensation of water vapor on its surface. The as-prepared ABAWH device extracts water vapor from the air by the CILs. The carbon nanotubes-modified cotton rods convert solar flux into thermal energy for freshwater production based on the interfacial evaporation process. Moreover, the thermal energy maintains the temperature of CILs inside the porous matrix at 25 °C regardless of the cold environmental temperature, and thus improved the water harvesting performance of the device. Notably, solar energy drives the water absorption and desorption simultaneously under solar irradiation. 1.49 kg per m^2 per day of water was collected by the as-prepared ABAWH device at a humidity of 30% under natural solar irradiation (solar intensity = 0.3–0.8 kW m^{-2}) with an environmental temperature of ∼6 °C. Additionally, the as-prepared ABAWH device exhibits stable water harvesting performance during the outdoor cycle experiment.

2. Experimental

2.1 Materials and chemicals

Commercial cotton rods were purchased from Taobao, China (density ≈ 0.17 kg m^{-3}). Unless otherwise noted, 1-hydroxyethyl-3-methylimidazolium chloride (C$_6$H$_{11}$N$_2$OCl, 99%, Adamas, China), lithium chloride (LiCl, 99%, Adamas, China) and ethanol (Sinopharm Chemical Reagent Co. Ltd., China) were used as received. Carbon nanotubes (CNTs, 4–6 nm, >98%) were purchased from Chengdu Organic Chemicals Co., Ltd. without any treatments. For all experiments, deionized water was used.

2.2 Fabrication of composited ionic liquids (CILs)

The composited ionic liquids (CILs) sorbent was fabricated by mixing 0.7 g [C$_2$OHmim]Cl and 0.3 g LiCl in 15 mL ethanol. A colorless solution was obtained by ultrasound. Then, the solution was put into a vacuum oven at 60 °C for 6 h until the ethanol was volatilized completely.

2.3 Fabrication of the CNTs-CILs@cotton rod

The CNTs-CILs@cotton rods were fabricated in the following steps: 50 mg carbon nanotubes dispersed in 15 mL CILs ethanol solution. A uniform suspension was obtained after ultrasound treatment. Then, the cotton rods with a desirable diameter and length were soaked into composites CILs and CNTs suspension. Finally, the modified cotton rods were dried in a vacuum oven at 60 °C for 6 hours.

2.4 Water vapor sorption/desorption experiment

The static and dynamic water uptake experiments with different temperatures and humidities were carried out in a constant temperature and humidity chamber (SUNCEK, HS-100) with high humidity uniformity (less than ±1.5% RH) and high temperature uniformity (less than ±0.5% °C) across the entire chamber. The mass change of the water sorption was measured
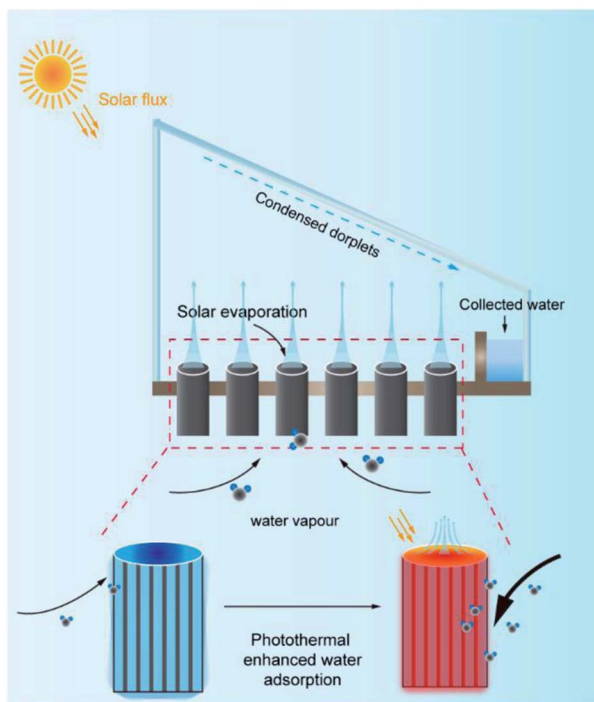

Fig. 1 Concept of freshwater production based on the CNTs-CILs@cotton rod device in cold climates.

by a high accuracy balance (ML204T, 0.1 mg in accuracy), which relayed information to a desktop computer in real-time. To test the water desorption of the CNTs-CILs@cotton rods, the CNTs-CILs@cotton rods first completed the water adsorption process by placing the cotton rods in the same desorption condition for 12 h. Then, the mass change of the wet CNTs-CILs@cotton rods were recorded under solar irradiation with various intensities.

2.5 Solar-to-thermal measurements of CNTs-CILs@cotton rod

The CNTs-CILs@cotton rod was put into a quartz glass chamber. The temperature inside the chamber was controlled by the circulating water. A solar simulator was placed above the chamber to simulate the solar light source. Thermistors were used to record the temperature change of the CNTs-CILs@cotton rod after solar irradiation.

2.6 Characterization

The SEM images were captured by a Hitachi S4800 FEG electron Microscope. The absorption spectra were characterized by a UV-vis-NIR spectrometer (Hitachi U4100). The temperature changes were recorded by thermistors (Hangzhou Xingxing Steel Shield Tools Co., Ltd.). The IR images were obtained by using a FLIR C2 camera. The mass change was measured by an electronic balance (FA2204N, Zhejiang Nade Scienic Instrument Co., Ltd.). The solar irradiation for indoor experiments was supplied by a solar simulator (CEL-APR250, Beijing China Education Aulight Co., Ltd.). The ionic concentrations in the condensed water were measured by inductively coupled plasma mass spectrometry (ICP-MS, iCAPRQ, Thermo Fisher Scientific).
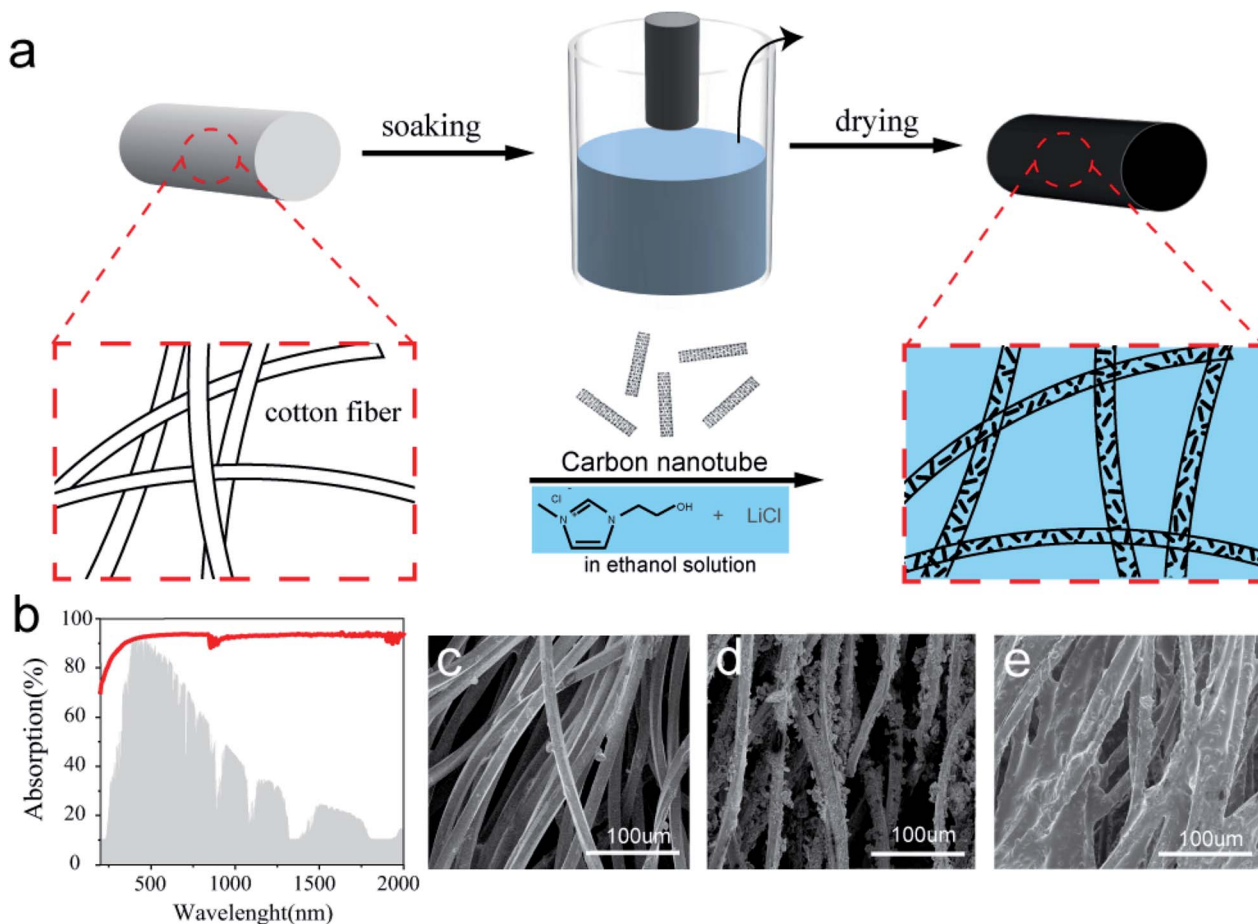
3. Results and discussion

3.1 CNTs-CILs@cotton rod characterization

The fabrication process of the CNTs-CILs@cotton rod is based on a physical impregnation method,[36] as shown in Fig. 2a. The optical photographs of the raw cotton rod, CILs-CNTs mixtures in ethanol solution and CNTs-CILs@cotton rod are shown in Fig. S1.† The UV-Vis-IR adsorption spectrum of the CILs-CNTs mixtures was measured (Fig. 2b). The suspension exhibits a strong adsorption of solar light in the wavelength range from 200 to 2000 nm. The average light absorption of the CILs-CNTs mixtures is around 93%. The reflection and transmission spectra of the CILs-CNTs mixtures are shown in Fig. S2.† The CILs-CNTs mixtures exhibited less light reflectance (<17%). The scanning electron microscope (SEM) images of the raw cotton rods, CNTs@cotton rod and CNTs-CILs@cotton rod are displayed in Fig. 2c, d and e, respectively. The images reveal that the commercial cotton rods are assembled by ultra-long cotton fibers with a diameter of 16 μm (show in Fig. S3†), forming an open porous network. Fig. S4† also present the EDS maps of the CILs-CNTs mixtures, which show that the mass ratio of LiCl in the CILs-CNTs mixtures is above 21%. These results are in good agreement with our experiment design. The surface area of the CNTs-CILs@cotton rod is 174 m² g⁻¹ (Fig. S5†). Additionally, cotton rods maintain their morphology after modification of
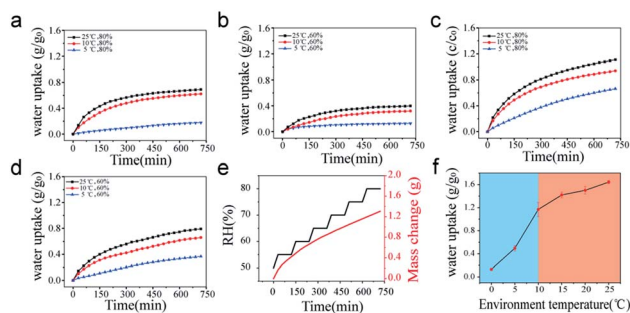
CNTs and CILs. Thus, we believe that the mesoporous structure of the cotton rods may offer a water vapor exchange pathway for the ABAWH devices. Moreover, the air in the mesoporous structure may decrease the heat loss of the photothermal materials under the solar irradiation, and thus increase the device performance in cold environments.

3.2 Atmospheric water sorption evaluation

In order to evaluate the water adsorption performance of the ILs based sorbent, we measured and compared the water uptake of the [C₂OHmim]Cl and CILs under different situations (static, dynamic temperature and humidity), according to those reported in the previous literature.[1] Fig. 3a and b display the static RH water absorption curves of [C₂OHmim]Cl at different temperatures. In the initial stage of 300 min water adsorption, the weight change of the [C₂OHmim]Cl increased rapidly, which indicated that there was a relatively fast water uptake. The water uptake rate then gradually decreased and reached the saturation point. The corresponding uptake rate of sorbents is shown in Fig. S6.† As shown in Fig. 3a, the mass changes of [C₂OHmim]Cl water uptake were finally recorded as $0.69 \ g \ g_0^{-1}$, $0.62 \ g \ g_0^{-1}$, and $0.18 \ g \ g_0^{-1}$ at environment temperatures of 25 °C, 10 °C and 5 °C at 80% humidity, respectively. A similar result was obtained at 60% RH (Fig. 3b). When the environment temperature was beyond 10 °C, the water uptake value changed subtly. However, when the environment temperature was below 10 °C, the water uptake value had decrease sharply. The uptake rate also fluctuated by temperature changes. The water uptake rate value increased by 20% when the temperature was raised from 10 °C to 25 °C, but the water uptake rate value decreased by 80% when the temperature dropped from 10 °C to 5 °C (Fig. S6†). It should be noted that the water uptake of the ionic liquid can be attributed to the diffusion of water molecules at the liquid/air interface, as well as in the ionic liquid, which was reported in the previous literature.[34] Thus, we believe that the decrease of environmental temperature will affect the diffusion rate of the water molecule. Accordingly, we speculate that the low temperature restrains the sorbent adsorption performance. Considering that the inorganic water absorber displayed larger adsorption capacity than the ionic liquids, a LiCl dosage was added to [C₂OHmim]Cl to improve the water adsorption performance of the liquid adsorber. The water adsorption performances of CILs ([C₂OHmim]Cl : LiCl = 5 : 5, 7 : 3, 8 : 2, respectively) are shown in Fig. 3c, d and S7.† It could be observed that the water adsorption performance of CILs was enhanced by increasing the concentration of LiCl in the mixture. However, the increased LiCl concentration led to the fluidity decrease of the mixture (shown in Fig. S8†). In view of the cotton rods being modified by CILs based on a dip-coating method, we finally chose CILs with a [C₂OHmim]Cl/LiCl ratio of 7 : 3 to optimize the water adsorption performance, as well as its fluidity. $1.21 \ g \ g_0^{-1}$ of water uptake was achieved by the optimized CILs when the humidity was 80%. Notably, the CILs exhibit larger water adsorption capacity than the liquid sorbents, as well as the water uptake rate, which were reported in the previous literature (as shown in Table S1†). The

Fig. 2 (a) Schematic illustration of the fabrication procedure of the CNTs-CILs@cotton rod. (b) UV-vis-IR absorption spectrum of the CNTs-CILs suspension. For comparison, the standard AM 1.5 G solar spectrum is also supplied in the gray area. (c) A typical SEM image of the commercial cotton rod, (d) a typical SEM image of the cotton rod modified with CNTs. (e) A typical SEM image of the cotton rod modified with CNTs and composited ILs.

Fig. 3 (a) The static water absorption curves of [C$_2$OHmim]Cl at different temperatures under 80% humidity, (b) 60%. (c) The static water absorption curves of CILs ([C$_2$OHmim]Cl : LiCl = 7 : 3) at different temperatures under 80% humidity, (d) 60%. (e) The dynamic RH water absorption of CILs at 25 °C. (f) Water adsorption of CILs at different temperatures.

improvement of the water adsorption capacity by the addition of LiCl could be according to the high interaction with water, while the higher water uptake rate is due to the faster water molecular exchange rate at the water–air interface offered by [C$_2$OHmim]Cl.[37,38] Meanwhile, the sorption performance of

CILs is the same as [C$_2$OHmim]Cl under an environmental temperature of 5 °C. The dynamic RH water absorption of CILs at 25 °C is shown in Fig. 3e. The water sorption started at a low humidity of 50%, and then gradually increased with the increase of humidity. It was shown that CILs had a broad sorption window. In Fig. 3f, we recorded the amount of CILs water uptake at different environmental temperatures under RH ∼80% after 24 h. The amount of CILs water uptake increased sharply with the increase of the temperature in a cold environment (in the range from 0 to 10 °C), while the value of the water uptake became stable when the environmental temperature was above 10 °C. These results suggested that the CILs for water harvesting from the air will exhibit better performance in a warmer environment. Hence, it is necessary to stabilize the working temperature of CILs beyond 10 °C to improve the ABAWH device performance.

3.3 Photothermal performance and water desorption of CNTs-CILs@cotton rod

The photothermal performance of the CNTs-CILs@cotton rod was investigated, as shown in Fig. 4. As a proof-of-concept, we

placed the CNTs-CILs@cotton rod in a double-glazing cavity glass chamber and recorded the temperature changes of the CNTs-CILs@cotton rod exterior ($T1$), CNTs-CILs@cotton rod interior ($T2$) and the environment ($T3$) under a solar intensity of 1 kW m^{-2}, respectively, as shown in Fig. 4a. Considering that the water adsorption may affect the temperature change in the CNTs-CILs@cotton rod, all of the CNTs-CILs@cotton rods used in this section were dried at 60 °C in the oven before the photothermal measurements. As shown in Fig. 4b, $T1$ and $T2$ of the CNTs-CILs@cotton rod increased rapidly and achieved 57 °C and 42 °C under solar irradiation at an environmental temperature of 25 °C, while $T1$ and $T2$ of the CNT-CIL@cotton rod reached 38 °C and 25 °C at 5 °C under the same condition (Fig. 4c). The photographs of the thermal probe are shown in Fig. S9.† This result indicated that the cotton rod could maintain a desirable working temperature of CILs sorbent under solar irradiation when the environmental temperature was below 10 °C. Additionally, the heat flow simulation was carried out to further understand the temperature distribution under solar irradiation at steady state by using numerical simulation software (FLUENT, the simulation details in Fig. S10†). As shown in Fig. 4d, the interior temperature of the CNTs-CILs@cotton rod decreased gradually along the axial direction of the cotton rod, which had a discernible difference between the condition without CNTs-CILs@cotton rod (Fig. S11†). The correlation between the interior temperature and the cotton rod length is displayed in Fig. 4d. Hence, the optimized cotton rod length is in the range from 30 mm to 50 mm. The corresponding IR image of the CNTs-CILs@cotton rod

is shown in the insets of Fig. 4d. Furthermore, the $T2$ of the CNTs-CILs@cotton rods with different aspect ratio was recorded under solar irradiation (as shown in Fig. 4e). The CNTs-CILs@cotton rod with a length of 30 mm exhibited the best photothermal performance compared to other cotton rods under the premise of loading sufficient adsorbent. Therefore, we chose the CNTs-CILs@cotton rod with a length of 30 mm as the building block of the ABAWH device.

Then, we investigated the water desorption performance of the CNTs-CILs@cotton rod under the same irradiation condition in Fig. 2. The CNTs-CILs@cotton rods were first placed at a chamber with constant temperature and humidity for 12 h to ensure a full water sorption. The mass increase of the CNTs-CILs@cotton rods after water sorption is displayed in Fig. S12.† The water-saturated CNTs-CILs@cotton rods were exposed under a solar irradiation with an intensity of 1 kW m^{-2} for water release. Meanwhile, we consider the water evaporation of the CNTs-CILs@cotton rod in the dark condition (Fig. S13†). As shown in Fig. 5a, the water release could achieve 5.3 kg m^{-2} (RH = 80%, temperature = 25 °C), 3.4 kg m^{-2} (RH = 80%, temperature = 10 °C), 2.4 kg m^{-2} (RH = 60%, temperature = 10 °C), respectively. The corresponding water release ratios were 86%, 74% and 73%, respectively. As seen in Fig. 5b, the water evaporation rate of the water-saturated cotton rod initially increased and then decreased. We believe that the decrease of the evaporation rate is due to the water content decreasing, which makes the continuous transport of water challenging in the numerous channels of CNTs-CILs@cotton rods. It is noteworthy that the maximum rate of water evaporation rate for the water-saturated cotton rod was up to 2.4 kg m^{-2} h^{-1}. Moreover, we tested the water desorption of the water-saturated cotton rod under different solar intensities at RH of 80% and
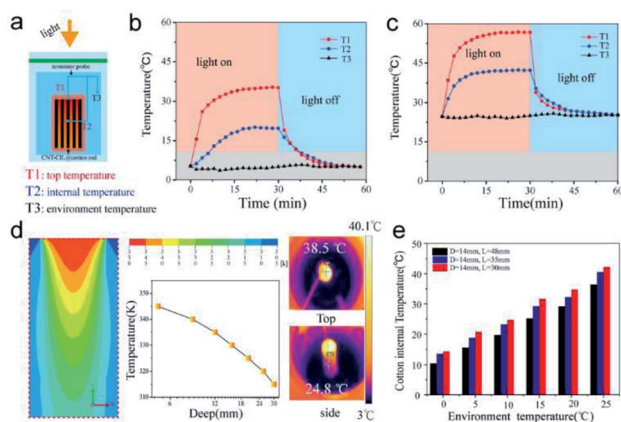

Fig. 4 (a) Illustration of the photothermal measurement. $T1$ is the temperature of the CNTs-CILs@cotton rod exterior under solar irradiation. $T2$ is the temperature of the CNTs-CILs@cotton rod interior under solar irradiation. $T3$ is the temperature of the environment. (b) The profile of the photothermal performance of the CNTs-CILs@cotton rod exterior under a solar intensity of 1 kW m^{-2} at 25 °C. (c) The corresponding photothermal performance of the CNTs-CILs@cotton rod at 5 °C. (d) The heat flow simulation image of the CNTs-CILs@cotton rod when $T1$ is 350 K. The curve is the temperature distribution with the cotton rod depth. The insets are the IR images of the CNTs-CILs@cotton rod in (c). (e) The correlation between the interior temperature and aspect ratio of the CNTs-CILs@cotton rod under solar irradiation. The diameter of the CNTs-CILs@cotton rods maintained their values, while their length changed.
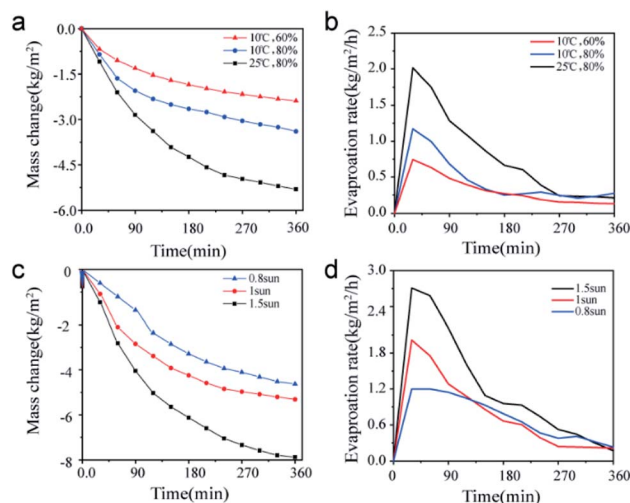

Fig. 5 (a) Mass change of the wet CNTs-CILs@cotton rod due to evaporation under a solar intensity of 1 kW m^{-2} at different temperatures and humidities. (b) The corresponding evaporation rate of the wet CNTs-CILs@cotton rod in (a). (c) Mass change of the wet CNTs-CILs@cotton rod due to evaporation at 80% RH and 25 °C under solar illumination with different intensities. (d) The corresponding evaporation rate of the wet CNTs-CILs@cotton rod in (c).

environmental temperature of 25 °C. The mass change of water desorption was 2.4, 3.4 and 5.3 kg m^{-2}, respectively (Fig. 5c), under solar intensities of 0.8, 1.0 and 1.5 kW m^{-2}. As displayed in Fig. 5d, the corresponding maximum water evaporation rate was 1.2 kg m^{-2} h^{-1}, 2.0 kg m^{-2} h^{-1}, and 2.7 kg m^{-2} h^{-1}, respectively, at the same condition of Fig. 5c. Notably, 75% of the absorbed water can be desorbed under a solar intensity of 0.8 kW m^{-2}. Furthermore, the evaporation rate of the CNTs-CILs@cotton rods is much higher than its water uptake rate, according to our results in Fig. 3 and S14.† Thus, we consider that the adsorbed water in the cotton network would be evaporated immediately under solar irradiation. The above results revealed that the CNTs-CILs@cotton rods exhibit considerable water absorption and desorption performance. Consequently, the as-prepared CNTs-CILs@cotton rods could be a potential candidate for the fabrication of the ABAWH device.

3.4 Outdoor measurement

Outdoor experiments were conducted to validate the feasibility of using the CNTs-CILs@cotton rods for ABAWH in practical application. The outdoor experiments were taken on the roof of our lab (WuHan, China. BD09 coordinate system is 114.164634, 30.51942, 18:30 December 31, 2020 to 16:30 January 1, 2021). Fig. 6a shows an optical image of the home-made ABAWH device for freshwater collection under natural environment and data recorder. As seen in Fig. 6b, the moisture sorption/desorption experiment was carried out from 9:00 to 16:30, where the ambient temperature, RH and solar intensity were traced per 15 min. The average temperature, RH and solar intensity were about 6 °C (under threshold temperature), 30% and 0.6 kW m^{-2}, respectively, in the daytime during our experiment. The IR image of the as-prepared ABAWH device at the outdoor condition is exhibited in Fig. 6c. The top temperature was 47.3 °C, while the side temperature was 32.8 °C. It was obvious that the temperature of the CNTs-CILs@cotton rod was higher than the ambient temperature. The hot water vapor could be naturally condensed on the device wall, where purified water generation was visibly manifested *via* the appearance of droplets, agglomeration and streaming (Fig. 6d). The ion concentrations (Li$^+$, Ca^{2+}, Cl$^-$) in condensed water were analyzed, as shown in Fig. 6e. The results demonstrate that the collected water is drinkable according to the drinking water standard reported in the previous literature.[30,39] The trace amounts of ions in the collected water may be attributed to the ions dispersed in the water microdroplets during the evaporation process. The mass change of the ABAWH device and corresponding condensate water were recorded at night and daytime, respectively. All of the CNTs-CILs@cotton rods used in the ABAWH device were dried at 60 °C overnight before the measurements. The ABAWH device was first placed overnight at outdoor condition (Fig. S15†). In Fig. 6f, it can be observed that the increase of the device mass was 1.894 g after water adsorption at night (18:00–6:30). Condensed water can hardly be collected during the night time because there was no solar evaporation in dark condition. In contrast, water absorption and solar evaporation occurred simultaneously at day time
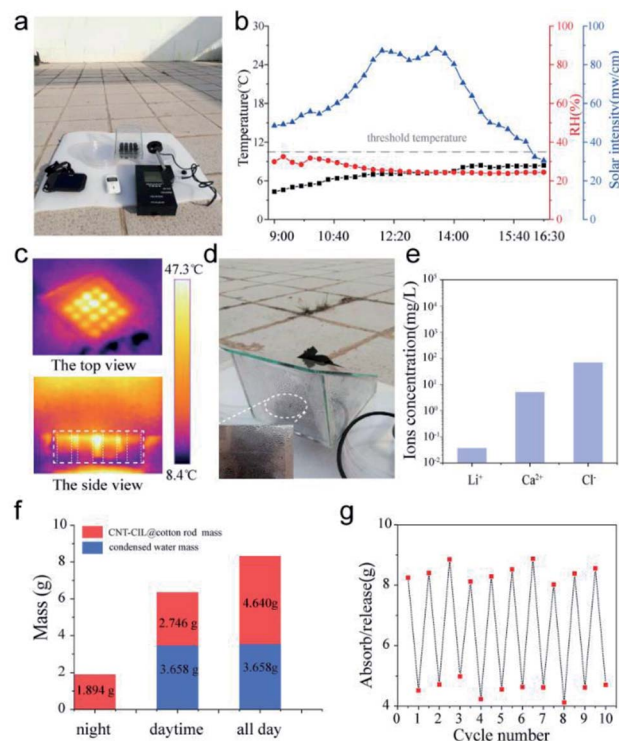

Fig. 6 (a) The optical image of the ABAWH device in the natural environment. (b) The variety of environmental temperature, relative humidity, and solar irradiation intensity changes during the practical solar-driven water evaporation. (c) The typical IR images of the CNTs-CILs@cotton rod device under solar irradiation during the water harvesting from the air. (d) The generated vapor could be naturally condensated into water droplets on the device wall. (e) The ions concentration of the collected condensate water. (f) The mass of the water adsorption - desorption of the as-prepared device at different time frames. (g) The stability of the as-prepared ABAWH device.

under solar irradiation. The increase of the device mass was 2.746 g, while the mass of the collected water was 3.658 g. The total water yield of the ABAWH device was 1.49 kg per m^2 per day after water harvesting for 24 hours. The stability of the ABAWH device is shown in Fig. 6g. The device maintained its water yield value after 10 times adsorption–desorption cycles under outdoor conditions (the average working temperatures were around 6 °C at daytime and 0 °C at nighttime). This demonstration revealed the fact that the ABAWH device based on the CNTs-CILs@cotton rod could extract water from the air in the cold winter. Importantly, the as-prepared ABAWH device could convert solar energy to thermal energy to drive the interfacial evaporation process and simultaneously maintain the temperature of the liquid sorbent at a desirable value to promote its water adsorption performance in a cold environment.

4. Conclusion

In summary, we fabricated a solar-driven adsorption-based atmospheric water harvesting device based on CNTs-CILs@cotton rods, which could hold the working temperature

of the liquid sorbent inside the device, improving the water sorption performance regardless of the change of the environmental temperature. The CNTs convert solar flux to thermal energy for generating vapor and heating liquid sorbent. The CILs sorbent is composed of [C$_2$OHmim]Cl and LiCl, which displayed better water absorption performance compared with other advanced liquid sorbents. The CILs present fast moisture absorption kinetics. CNTs and CILs are self-assembled on the surface of cotton fibers. The water vapor can exchange with the ambient air through the mesoporous structure of the cotton fibers. Moreover, the space in the mesoporous structure may decrease the heat loss of the photothermal materials under the solar irradiation, and thus hold the temperature inside the CNTs-CILs@cotton rods, as well as the device performance in the cold climate. We demonstrate that the CNTs-CILs@cotton rods-based ABAWH device extracts water from the air under outdoor condition (sunlight intensity is 0.3–0.8 kW m^{-2}, humidity was 30%, and environmental temperature is below 10 °C). 1.49 kg per m^2 per day of the water yield is obtained according to the outdoor experiments. The CNTs-CILs@cotton rod-based ABAWH can be synthesized easily using sustainable building blocks, could be readily manufactured on a large scale, is portable, and has superior AWH capability. It is therefore potentially useful for obtaining fresh water from air in water-scarce regions that are remote and landlocked, especially at cold climates.

Author contributions

Bolei Chen and Wenchang Zhang conceived the experiments and wrote the paper. Yu Xia carried out material fabrication and solar evaporation experiments. Zhaotong Wen finished the heat flow simulation. Wenxia Han, Shaofu Wang, Yiping Cao, Rong-Xiang He and Yumin Liu contributed to the analysis of the results. All of the authors contributed to revising the manuscript and approved the final version.

Conflicts of interest

There are no conflicts to declare.

Acknowledgements

Notes and references

1 S. N. Gosling and N. W. Arnell, Clim. Change, 2013, 134, 371–385.
2 M. M. Mekonnen and A. Y. Hoekstra, Sci. Adv., 2016, 2, e1500323.
3 J. F. Pekel, A. Cottam, N. Gorelick and A. S. Belward, Nature, 2016, 540, 418–422.
4 R. Li, Y. Shi, M. Alsaedi, M. Wu, L. Shi and P. Wang, Environ. Sci. Technol., 2018, 52, 11367–11377.
5 C. Chen, Y. Kuang and L. Hu, Joule, 2019, 3, 683–718.
6 M. Ejeian and R. Z. Wang, Joule, 2021, 5, 1678–1703.
7 S. Neto, in Water Challenges of an Urbanizing World, 2018, ch. 6, DOI: 10.5772/intechopen.72876.
8 R. I. Woolway, B. M. Kraemer, J. D. Lenters, C. J. Merchant, C. M. O'Reilly and S. Sharma, Nat. Rev. Earth Environ., 2020, 1, 388–403.
9 X. Han, L. Zang, S. Zhang, T. Dou, L. Li, J. Yang, L. Sun, Y. Zhang and C. Wang, RSC Adv., 2020, 10, 2507–2512.
10 K. Li, M. Gao, Z. Li, H. Yang, L. Jing, X. Tian, Y. Li, S. Li, H. Li, Q. Wang, J. S. Ho, G. W. Ho and P.-Y. Chen, Nano Energy, 2020, 74, 104875.
11 B. Chen, X. Zhang, Y. Xia, G. Liu, H. Sang, Y. Liu, J. Yuan, J. Liu, C. Ma, Y. Liang, M. Song and G. Jiang, J. Mater. Chem. A, 2021, 9, 2414–2420.
12 L. Shi, Y. Shi, S. Zhuo, C. Zhang, Y. Aldrees, S. Aleid and P. Wang, Nano Energy, 2019, 60, 222–230.
13 C. Zhang, H. Q. Liang, Z. K. Xu and Z. Wang, Adv. Sci, 2019, 6, 1900883.
14 R. Li, Y. Shi, M. Wu, S. Hong and P. Wang, Nano Energy, 2020, 67, 104255.
15 S. Zhuang, H. Qi, X. Wang, X. Li, K. Liu, J. Liu and H. Zhang, Global Challenges, 2021, 5, 2000085.
16 X. Zhou, H. Lu, F. Zhao and G. Yu, ACS Mater. Lett., 2020, 2, 671–684.
17 Y. Tu, R. Wang, Y. Zhang and J. Wang, Joule, 2018, 2, 1452–1475.
18 T. A. McHugh, E. M. Morrissey, S. C. Reed, B. A. Hungate and E. Schwartz, Sci. Rep., 2015, 5, 13767.
19 J. d. D. Rivera, Atmos. Res., 2011, 102, 335–342.
20 R. Chen, Z. Wu, T. Zhang, T. Yu and M. Ye, RSC Adv., 2017, 7, 19849–19855.
21 H. Kim, S. Yang, S. R. Rao, S. Narayanan, E. A. Kapustin, H. Furukawa, A. S. Umans, O. M. Yaghi and E. N. Wang, Science, 2017, 356, 430–434.
22 B. Chen, X. Zhao and Y. Yang, ACS Appl. Mater. Interfaces, 2019, 11, 15616–15622.
23 H. Kim, S. R. Rao, E. A. Kapustin, L. Zhao, S. Yang, O. M. Yaghi and E. N. Wang, Nat. Commun., 2018, 9, 1191.
24 F. Fathieh, M. J. Kalmutzki, E. A. Kapustin, P. J. Waller, J. Yang and O. M. Yaghi, Sci. Adv., 2018, 4, eaat3198.
25 H. L. Nguyen, N. Hanikel, S. J. Lyle, C. Zhu, D. M. Proserpio and O. M. Yaghi, J. Am. Chem. Soc., 2020, 142, 2218–2221.
26 K. Yang, T. Pan, I. Pinnau, Z. Shi and Y. Han, Nano Energy, 2020, 78, 105326.
27 H. Yao, P. Zhang, Y. Huang, H. Cheng, C. Li and L. Qu, Adv. Mater., 2020, 32, e1905875.
28 F. Zhao, X. Zhou, Y. Liu, Y. Shi, Y. Dai and G. Yu, Adv. Mater., 2019, 31, e1806446.
29 M. Wang, T. Sun, D. Wan, M. Dai, S. Ling, J. Wang, Y. Liu, Y. Fang, S. Xu, J. Yeo, H. Yu, S. Liu, Q. Wang, J. Li, Y. Yang, Z. Fan and W. Chen, Nano Energy, 2021, 80, 105569.

30 H. Qi, T. Wei, W. Zhao, B. Zhu, G. Liu, P. Wang, Z. Lin, X. Wang, X. Li, X. Zhang and J. Zhu, *Adv. Mater.*, 2019, **31**, e1903378.

31 X. Wang, X. Li, G. Liu, J. Li, X. Hu, N. Xu, W. Zhao, B. Zhu and J. Zhu, *Angew. Chem., Int. Ed. Engl.*, 2019, **58**, 12054–12058.

32 L. Cammarata, S. G. Kazarian, P. A. Salter and T. Welton, *Phys. Chem. Chem. Phys.*, 2001, **3**, 5192–5200.

33 Y. Cao, Y. Chen, L. Lu, Z. Xue and T. Mu, *Ind. Eng. Chem. Res.*, 2013, **52**, 2073–2083.

34 Y. Cao, Y. Chen, X. Sun, Z. Zhang and T. Mu, *Phys. Chem. Chem. Phys.*, 2012, **14**, 12252–12262.

35 Y. Chen, Y. Cao and T. Mu, *Chem. Eng. Technol.*, 2014, **37**, 527–534.

36 W. Ren, X. Tan, X. Chen, G. Zhang, K. Zhao, W. Yang, C. Jia, Y. Zhao, S. C. Smith and C. Zhao, *ACS Catal.*, 2020, **10**, 13171–13178.

37 Q. G. Zhang, N. N. Wang, S. L. Wang and Z. W. Yu, *J. Phys. Chem. B*, 2011, **115**, 11127–11136.

38 A. Maiti, A. Kumar and R. D. Rogers, *Phys. Chem. Chem. Phys.*, 2012, **14**, 5139–5146.

39 A. Entezari, M. Ejeian and R. Wang, *ACS Mater. Lett.*, 2020, **2**, 471–477.